

Under-ice acoustic navigation using real-time model-aided range estimation

EeShan C. Bhatt,^{1, 2, a} Oscar Viquez,² and Henrik Schmidt²

¹*MIT-WHOI Joint Program in Oceanography/Applied Ocean Science & Engineering,
Cambridge and Woods Hole, MA, USA*

²*Department of Mechanical Engineering, Massachusetts Institute of Technology,
Cambridge, MA*

(Dated: 20 February 2022)

1 The long baseline (LBL) underwater navigation paradigm relies on the conversion
2 of recorded travel times into pseudoranges to trilaterate position. For real-time op-
3 erations, this conversion has assumed an isovelocity sound speed. For re-navigation
4 in post-processing, computationally and/or labor intensive acoustic modeling may
5 be employed to reduce uncertainty driven by multipath arrivals. This work demon-
6 strates a real-time ray-based prediction method of the effective sound speed along
7 a path from source to receiver to minimize vehicle position error. This method was
8 implemented for a small scale AUV-LBL system in March 2020, in the Beaufort Sea,
9 in total ice-covered conditions and a double ducted acoustic propagation environ-
10 ment. The vehicle was successfully deployed and recovered. Given the lack of GPS
11 data throughout the vehicle’s mission, however, the pseudorange performance is first
12 evaluated on connections between GPS-linked beacons. The real-time ranging error
13 between beacons is roughly 11 meters at distances up to 3 km. But a consistent over-
14 estimation in the real-time method provides insights for improved eigenray filtering
15 by the number of surface bounces. An operationally equivalent pipeline is used to
16 re-position the LBL beacons and re-navigate the AUV, using a modeled, historical,
17 and a locally observed sound speed profile. The median re-navigation error is 1.84 ± 2.19 RMS m. The improved trilateration performance for suggests that this ap-
18 proach effectively extends the single meter accuracy of the deployed GNSS units into
19 the water column.

^aebhatt@whoi.edu

²¹ **I. INTRODUCTION**

²² Autonomous underwater vehicles (AUVs) are increasingly capable platforms to explore
²³ and sample the ocean, particularly for remote and/or dangerous regions. However, navi-
²⁴ gation uncertainty is a major challenge in considering AUVs as standard tools for oceano-
²⁵ graphic research. While land and air-based robots utilize information from Global Naviga-
²⁶ tion Satellite Systems (GNSS) to achieve stunning location accuracy and precision through-
²⁷ out the duration of their missions, AUVs cannot access GNSS fixes while underwater. There-
²⁸ fore, underwater vehicles have relied on any combination of dead reckoning, hydrodynamic
²⁹ models, inertial navigation systems, doppler velocity logs, and acoustic baseline positioning
³⁰ systems for navigation (Paull *et al.*, 2014). Limiting navigation error and drift requires an
³¹ AUV to periodically stall on the surface and obtain a GNSS fix to reset its position error.
³² This foolproof method of self-positioning is undesirable for stealth, adverse weather condi-
³³ tions, and mission efficiency, and inaccessible in a GNSS-denied situation like an ice-covered
³⁴ environment.

³⁵ Of underwater acoustic navigation systems, long baseline (LBL) is the most GPS-like
³⁶ in style and scale, and most appropriate for mitigating drift without overburdening com-
³⁷ putation or payload size on the vehicle (Van Uffelen, 2021). The state-of-the-art for LBL
³⁸ outsources depth to a pressure sensor and solves the two-dimensional localization problem
³⁹ with an isovelocity, linear scaling between one way travel time (OWTT) and range (Eustice
⁴⁰ *et al.*, 2006, 2007; Webster *et al.*, 2009, 2012). This assumption is valid for short scale
⁴¹ operations but oversimplifies propagation for larger and/or complex acoustic environments.

42 To achieve single meter, GNSS-like performance in a GNSS-denied environment, we demon-
43 strate an embedded ray-based data processing algorithm to convert recorded OWTTs into
44 pseudorange estimates. This methodology was integrated onto the AUV Macrura, deployed
45 and recovered in the Beaufort Sea, in March 2020, during the Ice Exercise 2020 (ICEX20).
46 A physics-driven methodology that received an *in situ* sound speed profile (SSP) was nec-
47 essary despite the small operational domain because of the relatively high-risk mission en-
48 vironment—total under-ice conditions and a variable double ducted acoustic environment.
49 For clarity, we delineate specific definitions for timing, positioning, and navigation from
50 [Howe et al. \(2019\)](#).

- 51 1. Timing is the ability to acquire and maintain accurate and precise time anywhere in
52 the domain of interest within user-defined timeliness parameters
 - 53 2. Positioning is the ability to accurately and precisely determine one's location refer-
54 enced to a standard geodetic system
 - 55 3. Navigation is the ability to determine current and desired position (relative or absolute)
56 and apply corrections to course, orientation, and speed to attain a desired position
57 anywhere in the domain of concern
- 58 Thus, navigation is inherently in real-time and depends on positioning; positioning depends
59 on timing. We also suggest re-navigation and re-positioning as post-processed corollaries,
60 which may include knowledge or processing capabilities not available *in situ*.

61 While RAFOS floats championed one way ranging for re-positioning ([Duda et al., 2006](#);
62 [Rossby et al., 1986](#)), the ability to do so for navigation was facilitated by the advent of

the WHOI Micro-Modem (Singh *et al.*, 2006) and synchronized clocks (Rypkema *et al.*, 2017). AUV navigation efforts have achieved root mean square (RMS) localization error on the order of tens of meters relative to GNSS surface position over less than ten kilometers in shallow (Claus *et al.*, 2018; Eustice *et al.*, 2007; Kepper *et al.*, 2017) and deep water (Jakuba *et al.*, 2008; Kunz *et al.*, 2008; Webster *et al.*, 2009). However, these efforts all used a nominal sound speed for travel time conversion and the vehicles were limited to shallower isovelocity regimes.

Localization algorithms that do consider environmental or acoustic uncertainty tend to focus on longer and larger experiments, where spatio-temporal variability cannot be ignored. These methods have also been reserved for post-processing as they can be labor intensive, computationally heavy, and/or require additional information like contemporaneous data. For example, gliders navigating with kinematic flight models and equipped with acoustic modems were later unambiguously associated with predicted ray arrivals, resulting in roughly a kilometer error and hundred meters uncertainty over basin scale propagation (Van Uffelen *et al.*, 2013). A follow up study investigated how a single temporally and spatially averaged SSP could mitigate position error for a four month glider mission (Uffelen *et al.*, 2016). Wu *et al.* (2019) cross correlate three days of real acoustic records with synthetic ones generated through ocean model snapshots from HYCOM (Chassagnet *et al.*, 2007). While potentially applicable for various ocean states, this is reliant on model realism and impractical for real-time operations. Mikhalevsky *et al.* (2020) introduces a “cold start” algorithm that does not require prior knowledge of track, position, or sound speed information. The algorithm inputs a four-dimensional ocean model, constrained by tomography data, into a range dependent

85 ray code to isolate the last path detected in a full multipath pattern. Then, a representative
86 group speed is solved for alongside position in a least squares fashion. This approach is able
87 to re-position a floating hydrophone array with an error of 58 m and a standard deviation
88 of 32 m based on six sources 129–450 km away but remains to seen for real-time navigation.

89 The ICEX20 AUV deployment necessitated an environmentally- and physically-driven
90 relationship between recorded travel times and estimated pseudoranges due to the multipath
91 uncertainty brought upon by an increasingly observed double ducted environment in the
92 Beaufort Sea, which some refer to as the “Beaufort Lens” ([Chen et al., 2019](#); [Chen and](#)
93 [Schmidt, 2020](#); [Litvak, 2015](#)).

94 Given that a lens introduces significant ray refraction, the Beaufort Lens is a convenient
95 shorthand for the spatio-temporal variability of the local temperature and sound speed
96 maxima generally around 50 to 60 m in depth. A neutrally buoyant layer of warm Pacific
97 Summer Water creates a unique double ducted environment —the upper duct degrades
98 signal coherence due to intensified ice interaction and the lower duct effectively traps sound
99 for long range propagation ([Poulsen and Schmidt, 2017](#)). Modeling output ([Duda et al.,](#)
100 [2021, 2019](#)) and experimental observations ([Ballard et al., 2020](#); [Bhatt, 2021](#)) suggest the
101 duct is persistent and widespread but not necessarily continuous; it and its acoustic effects
102 can be non-existent, minimal, or drastic. Transmissions in the upper duct, between the
103 surface ice and the lens, experience minimal attenuation but degrade in signal coherence
104 with repeated reflections under the ice. In lower duct, between the lens and its conjugate
105 depth in the Atlantic water, roughly 200 m, sound above 350 Hz is trapped effectively for
106 long range propagation ([Poulsen and Schmidt, 2017](#)).

107 Thorough reviews of uncrewed vehicle operations in polar environments can be found
108 in (Norgren *et al.*, 2014) and (Barker *et al.*, 2020); there is no comparable work in the
109 Arctic for a short range AUV deployment in the Beaufort Lens. Seminal (Bellingham *et al.*,
110 1995; Brooke, 1981; Hayes and Morison, 2002; Jackson, 1983; Light and Morison, 1989) and
111 more recent AUV deployments (Jakuba *et al.*, 2008; Kunz *et al.*, 2008; ?)(Fossum *et al.*,
112 2021; Kukulya *et al.*, 2010; Plueddemann *et al.*, 2012; Timmermans and Winsor, 2013; ?;
113 ?) witnessed the classical upward refracting sound speed profile that is amenable to an
114 isovelocity assumption.

115 Of note, despite different platforms and scales, are recent glider deployments in the
116 Canada Basin. In 2014, in partially ice-covered conditions, a long range LBL system with
117 WHOI Micro-Modems at 100 m exploited the lower duct for long range communication with
118 two gliders (Freitag *et al.*, 2016; Webster *et al.*, 2015). The sound speed value measured at
119 the time of reception was used to estimate range in post-processing. The beacon-to-beacon
120 performance was excellent, achieving contact at ranges greater than 200 km with a position
121 uncertainty of 40 m. The beacon-to-glider performance, however, deteriorated due to missed
122 contacts outside the duct. In 2017, gliders were deployed in a region with no ice coverage.
123 Ranges were linearly scaled by a statistical description of sound speed observations taken
124 during the experiment, 1450 ± 6.5 m/s (Graupe *et al.*, 2019). This resulted in an error
125 of 550 m, which was reduced by a factor between 4 and 5, depending on the dive, using a
126 post-processing acoustic arrival matching method. Both cases exploit the lower duct for high
127 fidelity communication at long ranges. Unintuitively, the smaller nature of our deployment
128 during ICEX20 is not a simplifying factor. For source depths typical to vehicle operations,

¹²⁹ 30 to 200 m, a shadow zone spans from 2 to 6 kilometers in range ([Schmidt and Schneider, 2016](#)).
¹³⁰

¹³¹ Compared to the previous small scale navigation efforts, the approach in this paper
¹³² integrates real-time model-aided data processing to estimate a representative sound speed
¹³³ along a path from source to receiver, leveraging climatology, *in situ* data, and fast acoustic
¹³⁴ modeling. The paper is organized as follows. Section [II](#) details the experimental conditions
¹³⁵ during ICEX20. Given that there is no GNSS ground truth for the vehicle position while
¹³⁶ underway, we first evaluate the real-time ranging performance of GPS-linked beacon-to-
¹³⁷ beacon communication events in section [III](#). Section [IV](#) uses insights from field data to
¹³⁸ introduce a new ray filtering algorithm to improve range estimation. Section [V](#) emulates the
¹³⁹ real-time processing pipeline to re-position beacon-to-beacon events and re-navigate AUV
¹⁴⁰ *Macrura*.

¹⁴¹ **II. OVERVIEW OF THE ICEX20 EXPERIMENT**

¹⁴² The results from this paper derive from data taken while deploying the AUV *Macrura*, a
¹⁴³ custom Bluefin-21, during the Ice Exercise 2020 (ICEX20), in the Beaufort Sea, from March
¹⁴⁴ 8 to 11, in double-ducted and ice-covered conditions. The AUV deployment was supported
¹⁴⁵ by the Integrated Communication and Navigation Network (ICNN) ([Randeni et al., 2020, 2021](#);
¹⁴⁶ [Schneider et al., 2020](#)), a specialized implementation of the LBL solution. The ICNN
¹⁴⁷ was initially developed via numerous virtual experiments to push the boundaries of algo-
¹⁴⁸ rithms and interfaces between different hardware components. The simulation approach
¹⁴⁹ serves as a testbed for robustness to produce better results than post-processing previous
¹⁵⁰ field data. The simulation capabilities are largely physics-driven with a modular system of
¹⁵¹ systems approach—an environmental simulator with sub-components for the ocean, includ-
¹⁵² ing Arctic ice drift and ocean acoustic propagation; a vehicle simulator with sub-components
¹⁵³ for vehicle dynamics and navigation; a topside hardware simulator and acoustic communica-
¹⁵⁴ tions simulator, both with a software-only configuration and a hardware-in-the-loop version
¹⁵⁵ ([Schneider and Schmidt, 2018](#)). The virtual environment similarly emulates the interfaces
¹⁵⁶ between the real components to test the entire software pipeline. Both simulation capabili-
¹⁵⁷ ties are integral to mission success.

¹⁵⁸ The ICNN is comprised of four ice buoys, in a loose rectangle, roughly 2 km away from a
¹⁵⁹ central ice camp with a topside computer, as shown in Fig. 1. The AUV and each ice buoy are
¹⁶⁰ outfitted with a WHOI Micro-Modem ([Singh et al., 2006](#)), with a four-element receiver array
¹⁶¹ and a single transmitter, one-tenth of a millisecond resolution. Acoustic messages were sent

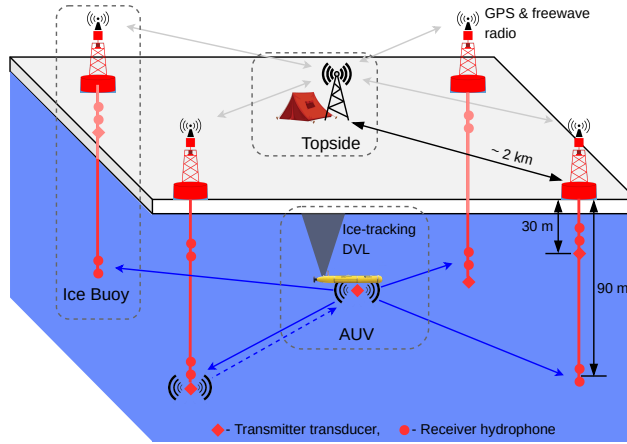


FIG. 1. A schematic overview of the Integrated Communication and Navigation Network (ICNN), which provides joint data-transfer and tracking between AUV and a human decision maker at Topside.

with a 10 kHz carrier frequency, 5 kHz bandwidth, and phase-shift keying (PSK) modulation on a thirty-second cycle, giving room for two-way communication throughout the mission volume. The receive and transmit elements were split between shallow and deeper depths (30 and 90 m, respectively) to provide better coverage across the shadow zone. While each buoy only has one transmit depth, all buoys have both receive depths but the active receive layer is consistent across all buoys. The design of the ICNN enables a self-adapting network to transmit and receive at the optimal depth to maintain contact with the AUV ([Schneider et al., 2020](#)). The buoys do not encompass the full horizontal range of the vehicle but are positioned to minimize overlap in trilateration for spherical positioning ([Deffenbaugh et al., 1996a](#)).

To balance competing uses of the acoustic channel, the network uses a single synchronized digital communication packet to provide both tracking and data to the operator.

174 1. The AUV, running an ice-tracking DVL and an onboard hydrodynamic model, broad-
175 casts its perceived location on a scheduled, time-synchronized message via WHOI
176 Micro-Modem

177 2. Four ice buoys, each outfitted with a WHOI Micro-Modem, receive messages from the
178 AUV and send that information over freewave radio to a Topside computer

179 3. The topside computer converts travel times into range estimates using a stochastic
180 embedded prediction of the horizontal group velocity via BELLHOP ray tracing code
181 ([Porter, 2011](#)) coupled with an updatable Virtual Ocean ([Bhatt et al., 2022](#); [Schneider](#)
182 and [Schmidt, 2018](#))

183 4. The topside computer calculates a new position by trilaterating the range estimates

184 5. The position differential, not the absolute position, is broadcast to the vehicle to
185 update its navigation solution and be robust to latency and intermittency

186 In the face of GNSS-denied navigation, this approach was anecdotally successful, as shown

187 in 2. The AUV *Macrura* was deployed through a hydrohole from an ice camp but recovered
188 through an emergency hydrohole. A random disk error stalled the AUV underneath the ice
189 but did not prevent it from transmitting its location. Due to an incoming storm, a team
190 placed a physical marker on the ice at the location. Three days later, *Macrura* was found

191 within a meter of the marker. We view the emergency recovery as qualitative proof of the
192 robustness of this navigation approach. Nonetheless, this paper specifically addresses the
193 third and fourth steps—the conversion of travel time into range and its effect on trilater-

194 ation. By focusing on range estimates between GPS-tracked beacons, and re-running the
 195 trilateration pipeline, the results are decoupled from all other mechanisms in the ICNN.

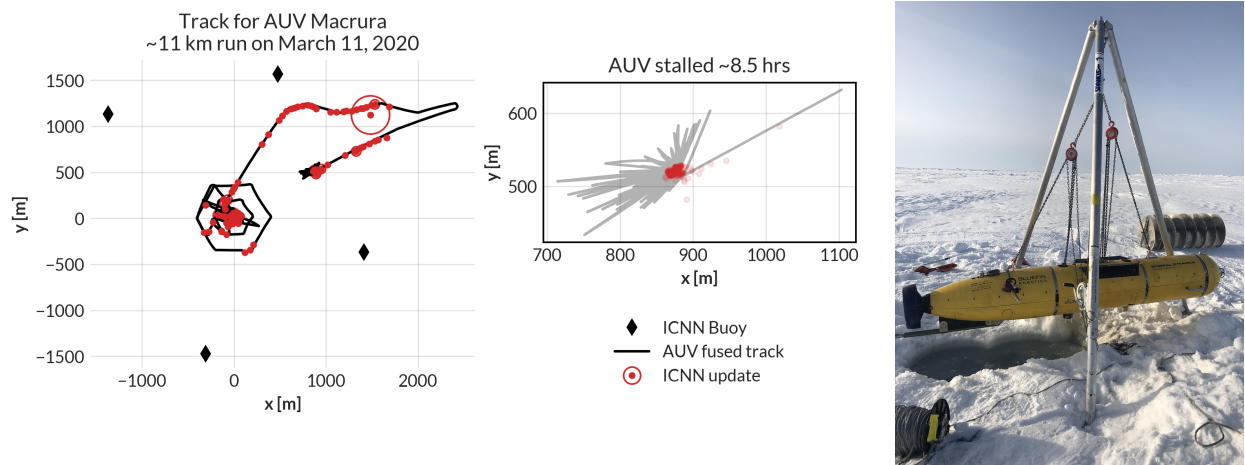


FIG. 2. The under-ice mission track for AUV Macrura, including the position updates as it stalled underneath the ice overnight. A marker was placed on the ice at the vehicle’s estimated self-location. It was recovered after a three day storm within a meter of the marker.

196 An important component to our navigation solution is an accurate estimation of the sound
 197 speed profile. Previous field experience, during the Ice Exercise 2016 (ICEX16), demon-
 198 strated the negative effects of the Beaufort Lens on tracking and communication ([Schmidt
 199 and Schneider, 2016](#)). Fig. 3 shows historical, modeled, and *in situ* data for both ICEX16
 200 and ICEX20. These three input streams were selected to mirror the information available
 201 on a submarine (personal conversation with LT B. Howard and LT CDR D. Goodwin).
 202 The SSP information was compressed with a basis representation and sent via lightweight
 203 digital acoustic message to the AUV ([Bhatt et al., 2022](#)). All modeled data comes from
 204 HYCOM ([Chassagnet et al., 2007](#)), which does not seem to capture the forcing mechanisms
 205 that cause the Beaufort Lens. For ICEX16, the data-driven profile was sourced from nearby

206 Ice Tethered Profilers (ITP) after the field experiment (Krishfield *et al.*, 2008; Toole *et al.*,
207 2011) and exhibits a fairly low lens; the historical profile is from the World Ocean Atlas.
208 For ICEX20, the chosen weights (data-driven) profile derives from a basis representation
209 estimation of initial CTD casts taken on site, showing an intense warm water intrusion; the
210 baseline (historical) profile, showing moderate ducted conditions, comes from the average
211 of March 2013 data. This month best matched sea ice and sound speed conditions at the
212 beginning of ICEX20 (Bhatt *et al.*, 2022). It is important to note that all profiles that do
213 show the Beaufort Lens do so with different local sound speed maxima at different depths,
214 reflective of the wide range of lens properties observed for all ITP data in the region. The
215 variability of the lens height and prominence is the main reason an updatable SSP was
216 integrated into the ICNN solution.

217 During ICEX20, the HYCOM profile was available but never deployed. For post-
218 processing comparison, we introduce both the HYCOM profile and an isovelocity case,
219 1441.8 ± 3.7 m/s, as the mean and standard deviation of the observed sound speed profile
220 over the first 200 m.

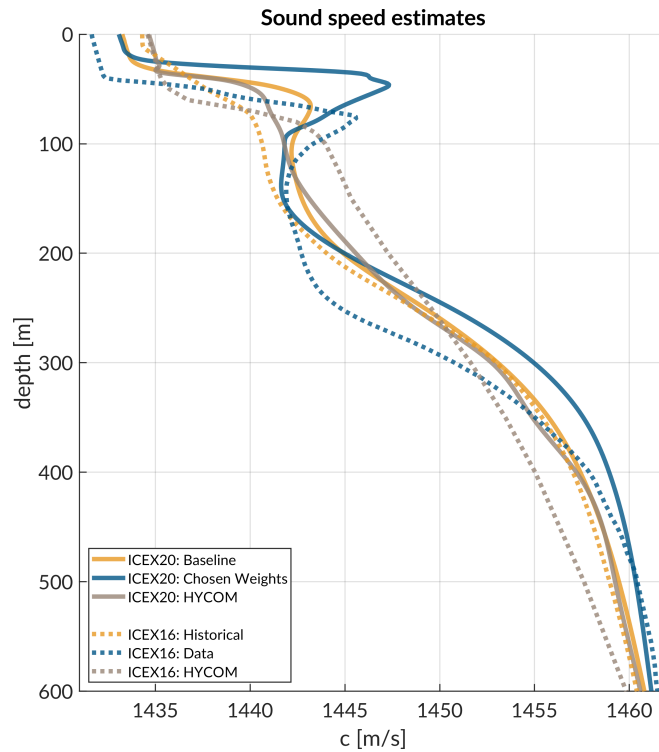


FIG. 3. Sound speed conditions for historical (baseline), data (chosen weights), and HYCOM model for both ICEX16 and ICEX20.

221 **III. REAL-TIME PSEUDORANGE ANALYSIS**

222 Because the vehicle's navigation solution during a mission can only be evaluated on the
223 basis of the error estimates sent, a sister experiment for validating the real-time ranging
224 approach was implemented. Ice buoy modems were run as "virtual vehicles" at a fixed
225 depth, receiving position updates from the other beacons as well as a camp site modem
226 lowered to 20 m. Figure 4 shows successful events sorted by source depth. In this analysis,
227 we assume there is insignificant displacement between the GNSS puck surface expression and
228 subsurface modem; this is supported by unusually low observed ice drift rates, on average,
229 just 0.7 cm/s.

230 **A. Minimal bounce criteria (MBC)**

231 The fundamental challenge to implement GNSS-like navigation, especially in an acousti-
232 cally complex propagation environment, is characterizing a single sound speed to compensate
233 for the effects of ray refraction and reflection. The use of the acoustic modem network for
234 tracking relies on the accurate estimates of travel times between the submerged platform
235 and LBL beacons, supported by clock synchronization and a pre-determined scheduling of
236 acoustic events. For the Beaufort Lens in particular, the strong multipath effects make it
237 virtually impossible to deterministically predict the modem's detected arrival time.

238 Instead, for each individual modem i , an embedded stochastic tracking framework is used
239 to provide a running estimate of the horizontal group velocity $u_{i,j}$ for the conversion from
240 travel time to range from modem j , with the ultimate goal of matching the naive group

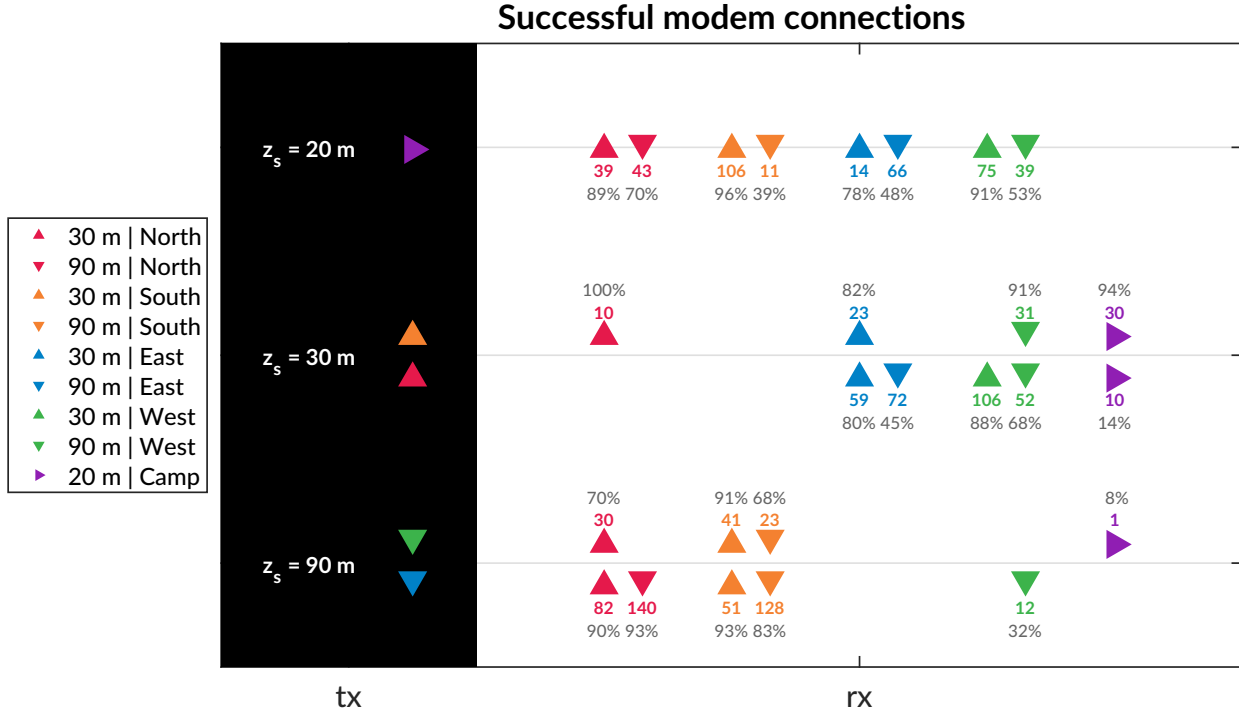


FIG. 4. An overview of the modem experiment by source and receiver depth and position with the number of successful decodings and the percent success rate, defined as the ratio of decoded to detected. The black column on the left, *tx*, shows the source depth, z_s . The column on the right, *rx*, shows the receivers with the amount of good contacts. The orientation of the triangles—sideways, upwards, and downwards—corresponds to depths of 20, 30, and 90 m.

²⁴¹ velocity, i.e. the GPS-recorded distance between two nodes divided by the modem-recorded
²⁴² one way travel time between them.

²⁴³ In the ICEX20 configuration, the acoustic tracking is running on the topside computer,
²⁴⁴ which controls the ICNN. Here we assume that the group velocities $u_{i,j}$ are smoothly varying
²⁴⁵ over the course of a vehicle mission, i.e., with respect to range, mission time, and the

²⁴⁶ frequency of updates relative to vehicle motion. The group velocity is tracked on a thirty-
²⁴⁷ second cycle using predictions from the *Virtual Ocean* infrastructure.

²⁴⁸ When the topside tracking framework receives a modem message, with a time delay, Δt ,
²⁴⁹ from one of the range modems, it will request a new estimate of the group velocity and its
²⁵⁰ associated uncertainty. The group velocity estimate is found using the vehicle's reported
²⁵¹ depth and the extrapolated navigation solution for range, \hat{r} , as inputs for the ray tracing
²⁵² program. The latter returns an impulse response estimate in the form of ray travel times
²⁵³ dt_j and amplitudes a_j for that range and depth.

²⁵⁴ The initial call to BELLHOP is over a local grid centered at the range and depth posited
²⁵⁵ by the onboard tracking solution. The grid, compared to a point solver, adds redundancy in
²⁵⁶ resolving the actual multipath structure for a reliable acoustic path without taxing onboard
²⁵⁷ computational time and memory. It is initialized as 11×11 points spanning 10 m horizontally
²⁵⁸ and 20 m vertically. The horizontal dimension reflects the accumulated position error given
²⁵⁹ a thirty-second communication cycle; the vertical dimension reflects how, computationally,
²⁶⁰ eigenrays of the same timefront seem to stack vertically in the water column. For each
²⁶¹ grid point, BELLHOP produces a number of arrivals resulting from multiple propagation
²⁶² paths for any source-receiver pair. Using only the N_0 rays with neither surface nor bottom
²⁶³ bounces, it will then estimate the current group velocity u from a power weighted average
²⁶⁴ of the ray travel times,

$$u = \frac{\hat{r} \sum_{n=1}^{N_0} a_n^2}{\sum_{n=1}^{N_0} dt_n a_n^2}, \quad (1)$$

265 and the associated weighted standard deviation,

$$\sigma_u \simeq \sqrt{\frac{\sum_{n=1}^{N_0} (dt_n - \hat{r}/u)^2 a_n^2}{\sum_{n=1}^{N_0} a_n^2}} \frac{u^2}{\hat{r}} \quad (2)$$

266 If no direct paths exist, i.e. $N_0 = 0$, then the group velocity is computed using the same
267 algorithm for the ray arrivals with one bounce, and so on.

268 Finally, the pseudorange is calculated simply as

$$r_{i,j} = u_{i,j} \Delta t_{i,j} \quad (3)$$

269 Thus the NBC method assumes the signal detected by the modem will be dominated
270 set of paths with the least number of boundary interactions. Importantly, this stochastic,
271 ensemble method for group velocity calculation can run in real-time, appearing to be orders
272 of magnitude faster than other post-processing methods which seek to determine the specific
273 ray itself that best matches a prominent indicator from the arrival structure. The BELLHOP
274 simulation that runs this calculation uses 3600 rays with launch angle fan of -60 to 60 degrees,
275 a representative depth dependent sound speed profile, and a range dependent bathymetry.

276 **B. Pseudorange error metrics**

277 The sister modem experiment generated 811 beacon to beacon communication events with
278 their own real-time MBC group velocity predictions. Given the complexity of the ICNN
279 system, this experiment did not collect an exhaustive set of data across all buoy, source
280 depth, receive depth, and sound speed combinations. The algorithm generally overestimates
281 pseudoranges because it resolves the effective sound speed for the most direct path.

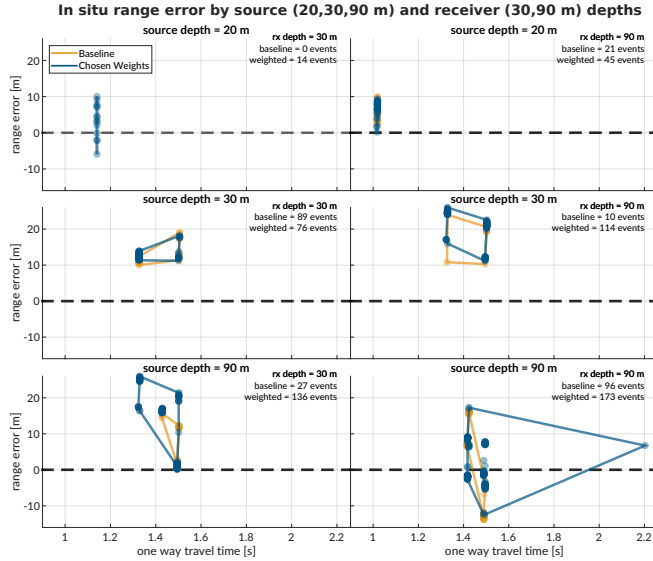


FIG. 5. The real-time range error by source (20, 30, and 90 m) and receiver (30 and 90 m) pairings for both sound speed estimates used during ICEX20. The amount of communication events is notated in the top right of each panel. The dashed line indicates no range error, and the boundary drawn indicates scope of the range error as a function of one way travel time.

282 Figure 5 shows the range error boundary for both SSP inputs used in ICEX20. A promising sign that the MBC method adapts sound speed realistically is no obvious error growth
283 as travel time increases. The baseline SSP ($n=243$ events) has an absolute pseudorange
284 error of 11.38 ± 4.23 m; the weighted SSP ($n=568$), 11.36 ± 8.12 m. The discrepancy
285 between these two is largely due to outlier events only contained in the weighted SSP set.
286
287 Where there is overlap between sound speed conditions used for the real-time MBC, the
288 pseudorange error difference is no more than a few meters. The overarching results show
289 that sound speed estimates derived from eigenrays for a local grid, as opposed to a singular
290 point, are accurate enough to support vehicle navigation. While the NBC looks for just the
291 least complex multipath, the high density of launch angles almost always guarantees a direct

²⁹² path. Nonetheless, the consistent overestimation of pseudorange invites further analysis into
²⁹³ acoustic arrival matching.

²⁹⁴ **C. Eigenray identification for beacon-to-beacon events**

²⁹⁵ Accounting for ice movement between beacons creates nominal ranges with small variabil-
²⁹⁶ ity. Figs. ?? each show eigenrays for three sound speed environments for source depths of
²⁹⁷ 20, 30, and 90 m, respectively. Eigenrays were initially found using the built-in BELLHOP
²⁹⁸ protocol with a launch angle step of 0.05 degrees from -60 to 60 degrees. Separately, recorded
²⁹⁹ travel times between beacons were clustered with 1 millisecond boundaries such that some
³⁰⁰ source-receiver pairs had multiple, distinct travel times to approximate. The BELLHOP
³⁰¹ eigenray returns were then filtered such that one was selected per travel time cluster, in the
³⁰² hopes that the eigenray will converge to the receiver locations for the most realistic sound
³⁰³ speed input. It should be noted that bottom bounces were recovered but filtered out. The
³⁰⁴ three source depths create distinguishable ray geometries with respect to the three sound
³⁰⁵ speed inputs.

³⁰⁶ **1. Source depth of 20 m**

³⁰⁷ For a source at 20 m in depth, shown in Fig. 6, reliable eigenrays are found for all sound
³⁰⁸ speed inputs. Rays refract upwards and neatly intersect with the shallow and deep receiver
³⁰⁹ locations between 1.5 and 1.8 km in range. However, the ray paths for the shallow receivers
³¹⁰ change both in the number of surface interactions and where the surface interactions occur
³¹¹ with respect to range across the SSPs. As the Beaufort Lens strengthens, the chosen paths to

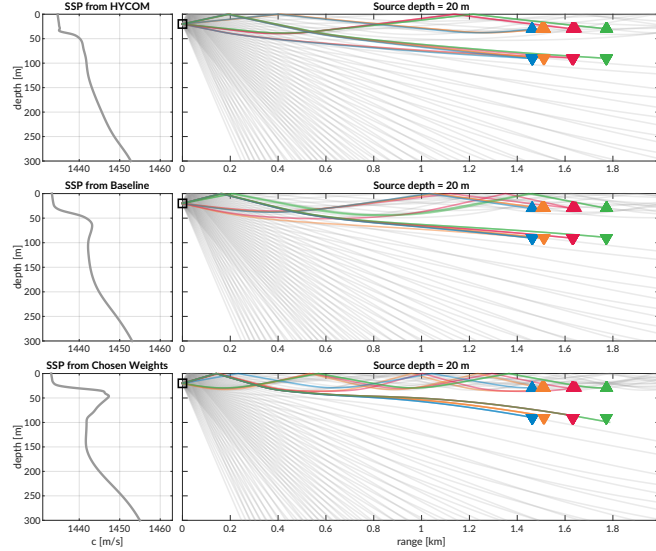


FIG. 6. Eigenrays for beacon to beacon events for each sound speed with a nominal source depth of 20 m. The beacons are highlighted in color/marker coding in Fig. 4. The eigenrays are curated from BELLHOP by travel time proximity and are traced in the representative receiver colors over a total ray fan in gray.

312 the second farthest shallow buoy (North, in red) interact with the surface more and become
 313 distinct. The weighted SSP shows the most interesting effects for the deeper receivers. The
 314 ray paths all interact with the surface and the eigenrays for the Northern (red) and Western
 315 (green) buoys are in fact the same ray.

316 **2. Source depth of 30 m**

317 The ray geometries from the 30 m source, shown in Fig. 6, show a similar degradation
 318 of eigenray identification with increased ducting. Receptions span 1.5 to 3.2 km. Once
 319 again, eigenrays for HYCOM and the baseline SSP are visually appropriate. Rays for the
 320 weighted SSP show how the surface channel intensifies ice interactions and how the shadow

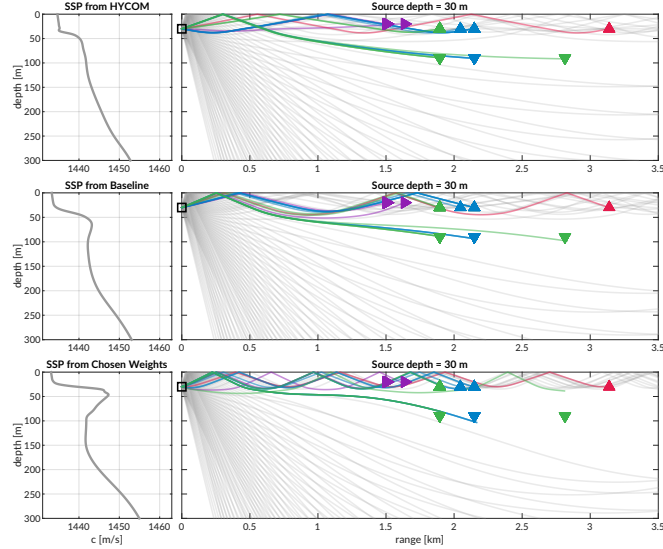


FIG. 7. Eigenrays for beacon to beacon events for each sound speed with a nominal source depth of 30 m. The beacons are highlighted in color/marker coding in Fig. 4. The eigenrays are curated from BELLHOP by travel time proximity and are traced in the representative receiver colors over a total ray fan in gray.

321 zone denies reliable acoustic paths. Pointedly, the increasing number of surface reflections to
 322 the farthest shallow buoy (North, in red) crystallize the MBC's tendency for overestimation.
 323 For the HYCOM, baseline, and weighted SSP inputs, the most appropriate eigenrays show
 324 2, 3, and 4 surface interactions.

325 ***3. Source depth of 90 m***

326 Lastly, Fig. 8 shows ray geometries from the 90 m source, elucidating a different extent
 327 of the shadow zone. While the receiver locations are similar to that of the 30 m source
 328 depth, the deeper source depth effectively negates the upper duct and places the upper (and
 329 some of the lower) receivers in unreliable acoustic paths. The HYCOM eigenrays still show

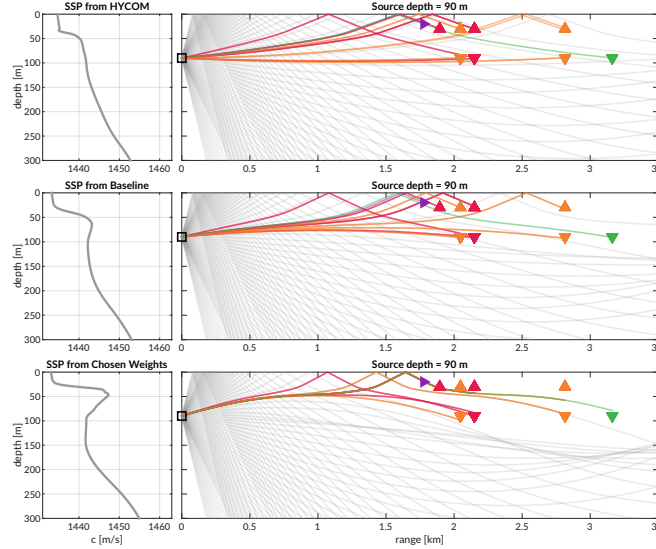


FIG. 8. Eigenrays for beacon to beacon events for each sound speed with a nominal source depth of 90 m. The beacons are highlighted in color/marker coding in Fig. 4. The eigenrays are curated from BELLHOP by travel time proximity and are traced in the representative receiver colors over a total ray fan in gray.

330 the most reliable acoustic paths that deteriorate with increasing ducted conditions. The
 331 lack of direct paths from the observed SSP further points out the shortcomings of the MBC
 332 approach.

333 The goal of the MBC algorithm was to provide a reliable, physically intuitive interpre-
 334 tation of the acoustic propagation without taking on the additional burden of regularly
 335 identifying specific paths that may connect any given source-receiver pair in the network.
 336 Its performance was adequate for vehicle navigation and would have likely sufficed if it were
 337 not for the prominence of the duct observed relative that of other model and data products.

338

³³⁹ **IV. POST-PROCESSED PSEUDORANGE ANALYSIS**

³⁴⁰ From all events recorded during the modem test experiment, there are 1242 successfully
³⁴¹ decoded beacon-to-beacon events. Only these events are used to evaluate ranging accuracy,
³⁴² as the ICNN was not configured to use receptions with failure flags. Thus, a post-processing
³⁴³ analysis that emulates the real-time navigation engine was run to overcome the unequal
³⁴⁴ distribution of communication events with respect to depth, range, and sound speed status.

³⁴⁵ It is important to note that the value for the extrapolated range, \hat{r} , is only tracked when
³⁴⁶ the modem runs the vehicle behavior; thus we replace \hat{r} with the GPS-tracked range for all
³⁴⁷ modem events. Because \hat{r} converges to the correct solution, a comparison of \hat{r} with the GPS-
³⁴⁸ tracked range shows a normal, zero-centered distribution within the bounds of GPS drift.

³⁴⁹ The present analysis therefore seeds realistic but “omniscient” knowledge of the extrapolated
³⁵⁰ range and leverages the post-processing pipeline to more thoroughly evaluate the acoustic
³⁵¹ range estimate for all modem events, with three relevant sound speed sources, and both
³⁵² group velocity criterion. Accordingly, the results in this section evaluate the utility of the
³⁵³ algorithms and sound speed sources, divorced from their role in the ICNN while maintaining
³⁵⁴ real-time relevance.

³⁵⁵ **A. Nearest bounce criteria (NBC)**

³⁵⁶ As shown in the eigenray traces of Fig. 7, the extent of ray bending and repeated
³⁵⁷ reflections is extremely dependent on the sound speed profile. An isovelocity approach
³⁵⁸ would completely miss this nuance; our field-tested approach that only resolved the simplest

359 path is unlikely to resolve the one that triggers modem detection. Based on this insight, a
 360 new algorithm, the nearest bounce criteria (NBC), is a slight modification from the MBC
 361 and includes multipath as a new dimension of information to exploit. This metric, while
 362 run in post-processing, adds a negligible amount of computation for real-time efficacy.

363 Given a running estimate for the horizontal group velocity $u_{i,j}$ between nodes i and j ,
 364 the navigation system has an extrapolated value for range, \hat{r} , and a recorded travel time,
 365 $\Delta t_{i,j}$. Instead of using only the N_0 rays with neither surface nor bottom bounces to estimate
 366 group velocity and subsequently moving to incremental number of bounces only when no
 367 valid direct path solutions exist, we solve for the power weighted average of the ray travel
 368 time for the N_k rays with k bounces,

$$t_k = \frac{\sum_{n=1}^{N_k} dt_n a_n^2}{\sum_{n=1}^{N_k} a_n^2}, \quad (4)$$

369 find the nearest matching power weighted average to recorded travel time,

$$t_{i,j,k} = \min_{k=0,1,2,\dots} |t_k - \Delta t_{i,j}| \quad (5)$$

370 predict a group velocity,

$$u_{i,j} = \frac{\hat{r}}{t_{i,j,k}} \quad (6)$$

371 and estimate the range as was done previously.

$$r_{i,j} = u_{i,j} \Delta t_{i,j} \quad (7)$$

372 This method selects a different group velocity based on the multipath arrival structure,
 373 as the detected arrival is not always the first arrival or the direct path and could even be
 374 masked by noise or blocked temporarily (Deffenbaugh *et al.*, 1996b). We manually cap the

375 number of bounces to 4 because of the smaller operational scale and the attenuation accrued
 376 with many surface interactions. Bottom bounces are not encoded separately because of ray's
 377 tendency to refract upward, not due to information limitations.

378 **B. Effective sound speed predictions**

379 The minimal and nearest bounce algorithms are applied with the three sound speed inputs
 380 shown in Fig. 7. The resulting predicted group velocities for all source depths are shown in
 381 Fig 9.

382 The goal of the group velocity estimation is to converge towards the implied sound speed,
 383 i.e. the GNSS-derived range divided by the recorded travel time. For a 30 m receiver depth,
 384 the NBC shows more overlap with data-derived values as it classifies multipath more cor-
 385 rectly. For a 90 m receiver depth, the overlap is less accurate due to computational con-
 386 straints of a limited fan of rays entering the shadow zone rendering a less reliable simulated
 387 times of arrival packet.

388 As the environmental and ray filtering method become better representations of the real
 389 ocean, the lower the expected mismatch is between the implied and estimated effective
 390 sound speeds. Analysis shows that the higher multipath classification produces more ac-
 391 curate sound speed predictions, likely driven by a tighter and/or sparser bundle of rays.
 392 However, that data are too small to draw significant conclusions. Discontinuities in mul-
 393 tipath classification verify our hypothesis for its importance to a smoothly varying group
 394 velocity, as shown in the cluster for a receiver depth of 30 m, where HYCOM jumps from

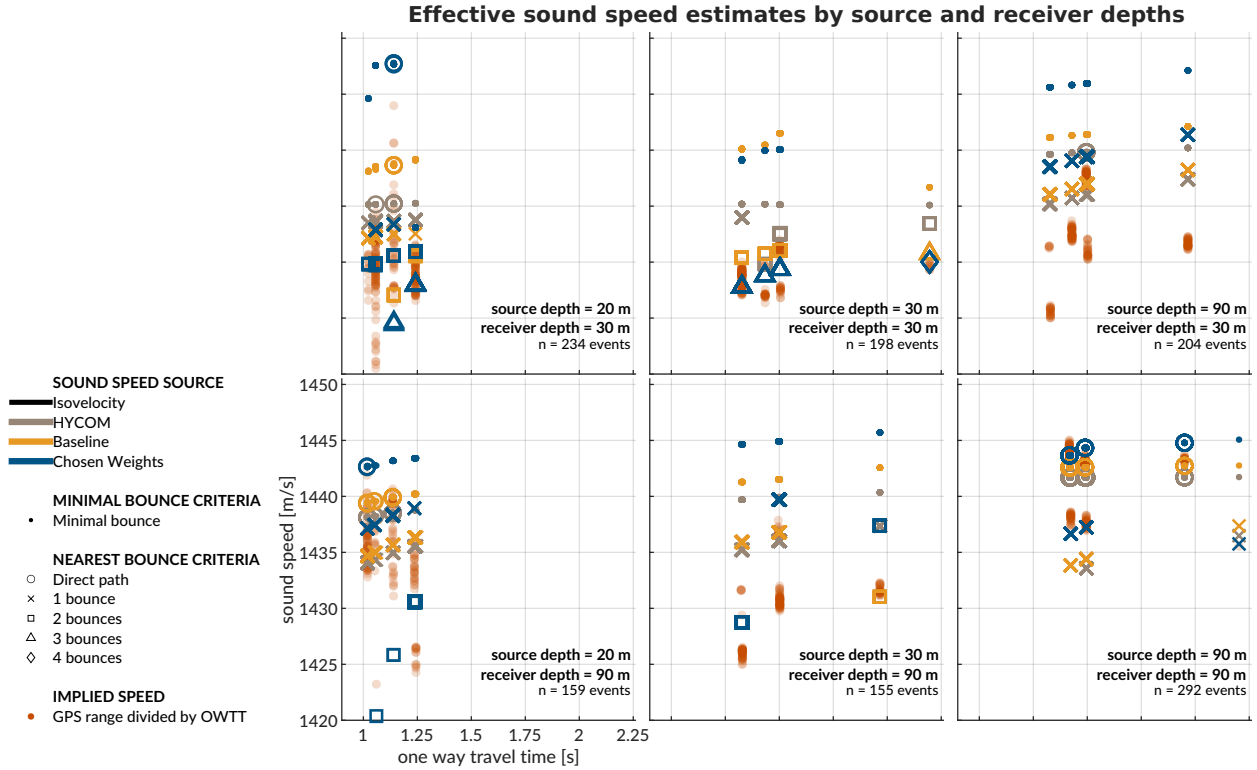


FIG. 9. A comparison of group velocity predictions for all beacon to beacon events in post-processing with a source depth of 30 m, with group velocity on the y-axis and recorded travel time on the x-axis. The left panel is for a receiver depth of 30 m; the right panel for 90 m. The sound speed source is indicated by color. The minimal and nearest bounce criterion are distinguished by different marker shapes, compared to the separately colored red dots showing the naive, data-driven group velocity calculation.

395 one to two bounces amidst the baseline SSP and weighted SSP smoothly increasing while
 396 consistently seeing two and three bounces, respectively.

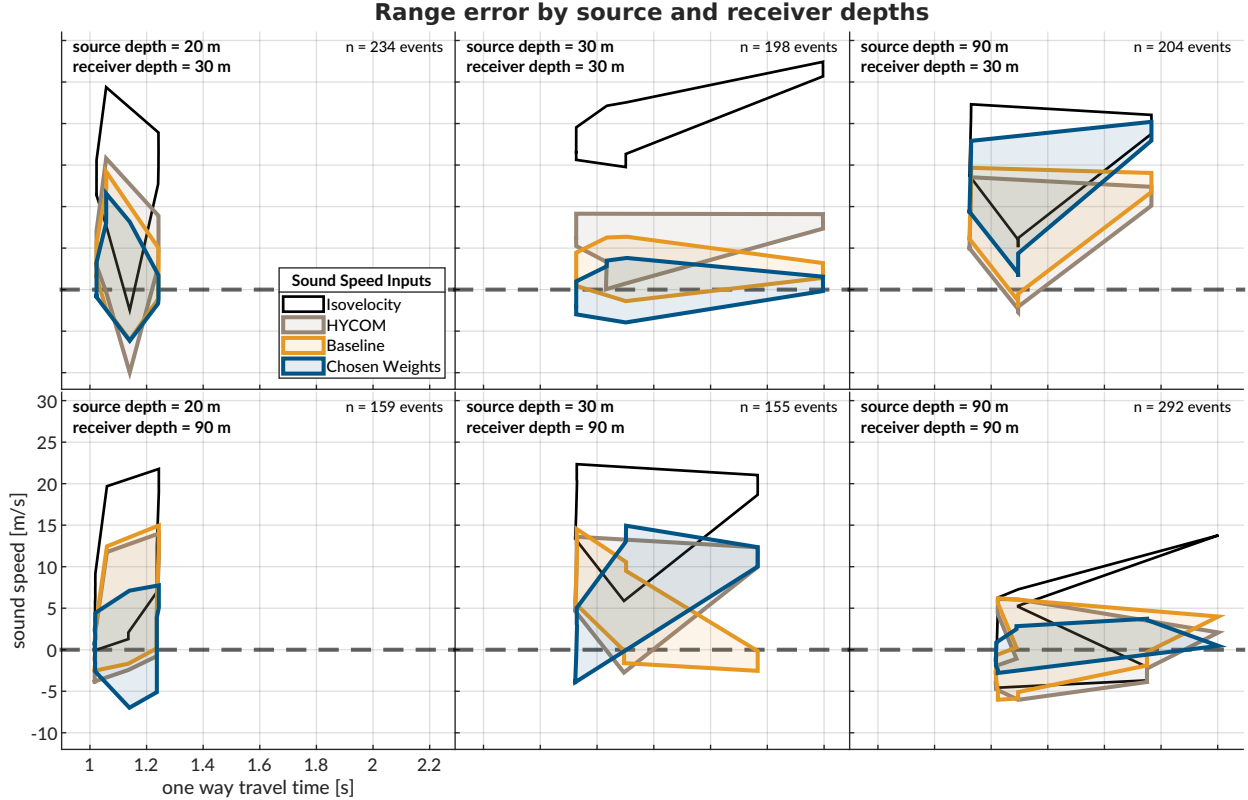


FIG. 10. The post-processed range error for source depths of 20, 30, and 90 m, and receiver depths of 30 and 90 m. The dashed gray line shows no error. The shaded region connects the range performance across all events.

397 **C. Pseudorange error metrics**

398 Fig. 10 shows the directional range error footprints for all three sound speed inputs with
 399 respect to OWTT, separated by source and receiver depth configurations. The weighted
 400 SSP range error generally has the smallest and most zero-centered footprint. The one case
 401 it does not is for the source-receiver pairings between 30 and 90 m in depth. The increased
 402 error for these reciprocal transmission paths is most likely driven by the computational
 403 artifacts encountered when propagating through the steep sound speed gradients of the lens

⁴⁰⁴ and through the shadow zone. All other source depth pairings are significantly improved
⁴⁰⁵ using the chosen weights compared to HYCOM or the baseline.

⁴⁰⁶ When using a linear scaling to convert travel time into range, any offset between the
⁴⁰⁷ assumed sound speed and the horizontal group velocity produces unconstrained error with
⁴⁰⁸ increasing receiver distance. Most importantly, we see the consequences of the adaptive
⁴⁰⁹ group velocity in that range error does not strictly increase with OWTT.

⁴¹⁰ The improvement from MBC to NBC is most evident for the realistic sound speed; while
⁴¹¹ the HYCOM SSP improves from a median absolute range error of 6.41 to 4.61 m, the
⁴¹² baseline SSP improves from 10.30 to 2.27 m, and the weighted SSP improves from 13.28
⁴¹³ to 2.12 m. Table I shows further statistics on the absolute range error by SSP and group
⁴¹⁴ velocity algorithm. The order of magnitude improvement in the ducted SSPs demonstrate
⁴¹⁵ the effectiveness of the algorithm exploiting the multipath conditions.

⁴¹⁶ As shown in table I, there is a striking maximum range error of 1491 m for the weighted
⁴¹⁷ SSP in the minimal bounce criteria. There are 10 events from South transmitting at 30 m
⁴¹⁸ depth to North receiving at 30 m depth. The OWTT spread is from 2.1958 to 2.1963 s; the
⁴¹⁹ naive group velocity is 1429.3 to 1430.1 m/s; and the GPS-tracked range is from 3138.54 m
⁴²⁰ to 3140.87 m. This example ends up being an excellent case study for how sound speed and
⁴²¹ multipath fidelity work in concert to minimize range error. The large error in this instance
⁴²² is driven by the MBC unexpectedly defaulting to a bottom bounce with a much greater
⁴²³ OWTT. The NBC classifies the multipath as 4 bounces, reducing the range error from
⁴²⁴ greater than a kilometer to less than a meter. While there is no actual way of knowing if
⁴²⁵ this is the correct multipath structure, the range error is remarkably small, at 0.025%. This

	Baseline		Chosen Weights		HYCOM	
	MBC	NBC	MBC	NBC	MBC	NBC
minimum [m]	0.01	0.00	0.00	0.00	0.11	0.01
25th % [m]	4.96	0.99	6.26	0.95	3.30	2.25
median [m]	10.30	2.27	13.28	2.12	6.41	4.61
75th % [m]	15.81	5.51	19.75	4.11	10.92	7.46
maximum [m]	22.52	14.96	1491	20.21	19.55	15.81

TABLE I. A comparison of range estimation metrics for each sound speed source and group velocity estimation algorithm for all 1283 beacon to beacon events via post-processing. The 0th (minimum), 25th, 50th (median), 75th, and 100th (maximum) percentiles are shown to the range resolution afforded by the WHOI Micro-Modem. There are a few outliers that drive the mean to be higher than the median.

426 pattern of not choosing the minimal observed bounce structure is consistent across all SSPs;
 427 the baseline goes from 1 to 3 bounces and HYCOM goes from 0 to 2 bounces. Notably,
 428 the baseline and HYCOM range errors are never egregiously large, but are nonetheless
 429 improved with the NBC algorithm. Thus, for acoustically complex environments, the NBC
 430 has a disproportionately positive impact as the estimated SSP approaches the desired SSP.

⁴³¹ **V. TRILATERATION FOR ICEX20 FIELD DATA**

⁴³² To overcome potentially intermittent acoustic communication, the operational paradigm
⁴³³ of the ICNN computes corrections relative to the trilaterated position estimates transmitted
⁴³⁴ by the vehicle, rather than transmitting the updated positions themselves. The reliability
⁴³⁵ of the correction is directly linked to how accurately the travel time measurements are
⁴³⁶ converted to pseudoranges. This section aims to resolve that tension by reevaluating the
⁴³⁷ trilateration results with respect to the MBC and NBC algorithms. The MBC/NBC sound
⁴³⁸ speed estimates were tracked independently for each transmitter-receiver pair; although the
⁴³⁹ sound speed was expected to be locally smooth near a given receiver, no such assumption
⁴⁴⁰ was enforced between distinct acoustic links.

⁴⁴¹ **A. Re-positioning beacon to beacon events**

⁴⁴² When the beacons ran as virtual vehicles, the ICNN did not have access to that buoy's
⁴⁴³ GPS data stream except for what was sent via digital acoustic message. The static nature of
⁴⁴⁴ the experiment means that the initial estimate transmitted to the ICNN was in fact a ground
⁴⁴⁵ truth position. Therefore, a distribution of corrections from the ICNN, as shown in Fig. 11,
⁴⁴⁶ reflects positioning accuracy. The NBC clearly outperforms the MBC, with almost 80% of
⁴⁴⁷ the corrections below 6 meters and the median within the deployed GNSS puck precision
⁴⁴⁸ of 3 meters. By contrast, the MBC shows roughly 20% within the GNSS puck precision,
⁴⁴⁹ and separate peaks from 9–12 meters and 21–27 meters. This trimodal nature reflects the
⁴⁵⁰ distribution of reflections on the ice surface.

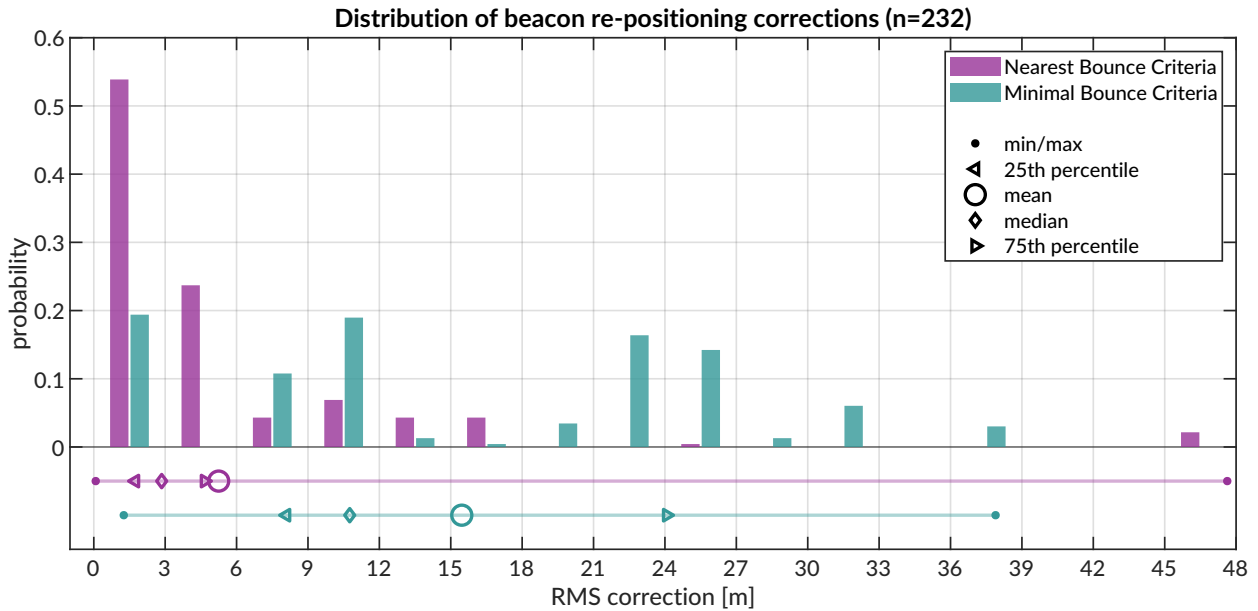


FIG. 11. Trilateration events; however, 264 entries are 2-beacon solutions, 22 are 3-beacon, and 2 are 4-beacon. When limited to only two ranging circles, the trilateration chooses the closer of the two intersection points. The x-axis is cut off at the upper limit for the NBC algorithm.

451 In several events, the MBC is unable to accurately estimate the effective sound speed for
 452 one of the acoustic links, leading to a large positioning error. The NBC, however, better
 453 resolves an approximation of the acoustic path. For example, in some trilateration solutions
 454 for the Eastern buoy, the MBC shows a correction of more than a kilometer; the NBC is
 455 two order of magnitudes less.

456 **B. Re-navigating AUV Macrura**

457 Up to this point, pseudorange estimation and localization have been evaluated on GPS-
 458 linked beacon-to-beacon connections to validate the NBC algorithm. This analysis ports the
 459 MBC and NBC algorithms to re-navigate the AUV *Macrura*.

460 The AUV dataset clearly exhibits instances where a receiver detects the same transmission
 461 more than once. This is not surprising considering the complex multipath provided by
 462 the Beaufort Lens. The 11 hour vehicle mission contains 3260 transmissions, 12938 total
 463 detections, and 4704 successful receptions. Allowing receptions with PSK errors would
 464 almost double the number of recorded multipath arrivals exploited for positioning, if a real-
 465 time solution could correctly parse paths from different arrivals in the same thirty-second
 466 cycle. Thus it remains a future endeavor to explore how failure mode information from
 467 acoustic modems could be used to identify unsuccessful but otherwise trustworthy arrivals
 468 to augment trilateration samples.

469 The following performance analysis is constrained to what the vehicle acted on in real-
 470 time. AUV *Macrura* and the ICNN ran an adaptive depth behavior to maintain acoustic
 471 communication on the insight that cross-layer links were more likely to fail than same-layer
 472 ones. Accordingly, the vehicle dove deeper than 50 meters about 20% of the time it was
 473 underway.

474 In contrast to the modem tests, where position correction illustrated re-positioning ac-
 475 curacy, the re-navigation corrections are less valuable in the absence of GNSS ground truth.
 476 The correction magnitude necessarily depends on the vehicle's internal navigation estimate,
 477 which is prone to larger errors from sensor drifts, ocean currents, and other error not cap-
 478 tured in the hydrodynamic model. Thus, larger corrections are not necessarily indicative of
 479 worse performance. Navigation accuracy may be better described by trilateration error, the
 480 RMS of the remaining pseudorange errors from each acoustic link.

481 Fig. 12 shows the correction magnitudes and trilateration errors for events with three or
 482 more receptions during AUV operations. Whereas the MBC has a fairly bimodal nature,
 483 with peaks centered around 10–15 and 35–40 m, the NBC favors smaller corrections, from
 484 5–20 m, and has a long tail. The distribution of corrections are much larger than the
 485 distribution of RMS error. It is apparent that, while both methods are quite successful,
 486 there is strong evidence that the NBC achieves single meter accuracy.

487 C. Investigating potential GNSS noise

488 The fact that the bulk of the best performing re-navigation error exists within the pre-
 489 cision of the GNSS unit deployed invites a further look into GNSS noise. In the Arctic,
 490 GNSS performance worsens due to poor constellation coverage, larger ionospheric effects,
 491 and multipath interference. The National Security Implications of Climate Change for U.S.
 492 Naval Forces (Council, 2011) details some of the limitations of the Global Positioning Sys-
 493 tem (GPS) at polar latitudes. Radio infrastructure that provides position corrections and
 494 references does not regularly extend to polar regions. The effect is minor for surface platform
 495 navigation —roughly 15 m of horizontal precision has been displayed at the North Pole—but
 496 is significant enough to register against the modem’s detected travel times. Figure 13 zooms
 497 in on the GNSS and OWTT noise relative to the ice movement for two pairs of modem buoy
 498 connections. The two panels indicate the GPS drift as $\delta R = \sqrt{\delta x^2 + \delta y^2}$ and temporal drift,
 499 δt , relative to the median OWTT recorded between the two modems. The dashed line is
 500 scaled by a group velocity of 1440 m/s, such that if there were ideal sensor measurements
 501 with no drift, all events should exist on or near the line.

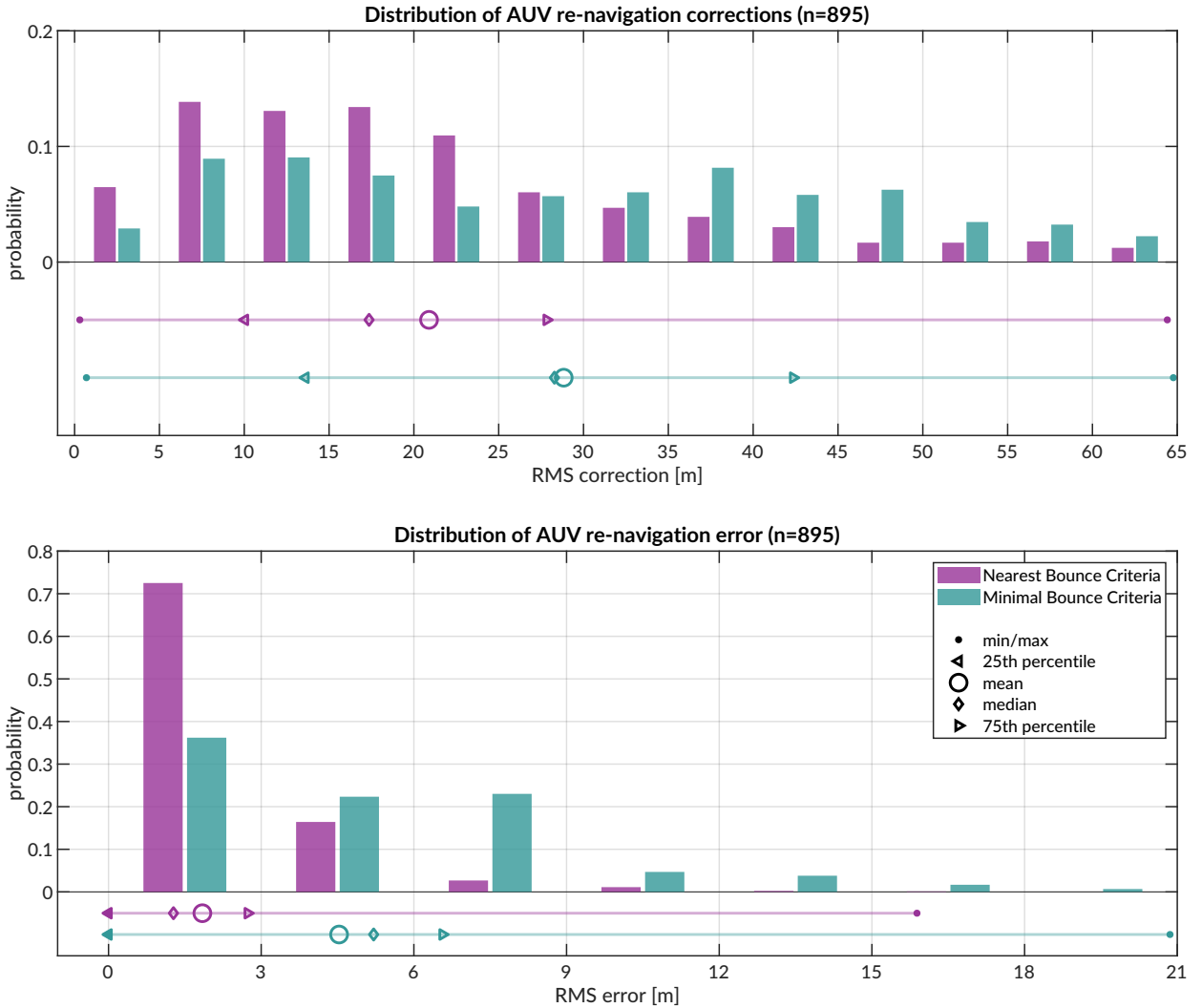


FIG. 12. Distribution of vehicle re-navigation corrections (top) and error (bottom) computed in post-processing for the Minimum and Nearest Bounce Criterion.

502 The top panel shows the connections between the North and East buoys. There is rela-
 503 tive, i.e. non-rigid, ice movement between the North and East buoys, evidenced by events
 504 spanning the dashed line. But the height of the scatter plot is indicative of the precision of
 505 the GPS signal, as it remains consistent across many arrival time bands. Naturally, some
 506 minor offsets between these vertical bands relate to different operational configurations of

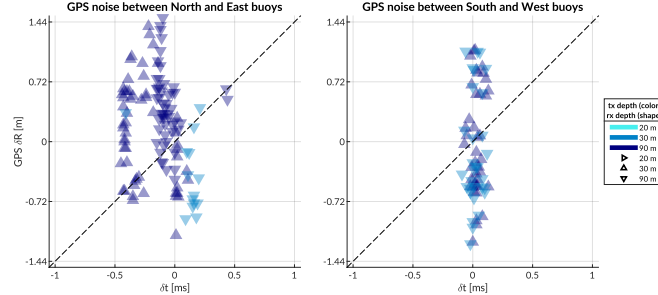


FIG. 13. A comparison of GPS drift (y-axis) versus OWTT drift (x-axis), colored by source and receiver depth. The physical link between North and East are shown on the top; South and West is on the bottom.

507 source and receiver depth. However, the large majority of events show vertical banding for
 508 the same nominal δt , indicating the amount of GPS drift.

509 This idea of GPS drift relative to the same OWTT measurements is further indicated by
 510 events between the other two buoys, South and West, in the bottom panel. These buoys are
 511 moving in a more rigid ice floe and there is minimal impact by source and receiver depth
 512 on the spread of OWTT. The GPS drift is much larger relative to the OWTT drift, which
 513 is sensitive to acoustic scattering, multipath, and/or environmental microstructure.

514 These are just two subsets of the physical links that cover all four GPS modem buoys. The
 515 GPS at camp is the least accurate due to the human activity and infrastructure occluding
 516 the physical puck.

517 VI. DISCUSSION

518 Given the computational constraints of real-time modeling, the gridded approach facil-
 519 itates enough multipath classification to build in a “ray ensemble” of characteristic group

520 velocities. This result is not always possible when aiming to find eigenrays to just an individual point, even with a higher density of launch angles. An important takeaway for those
521 interested in ray-based localization is leveraging a local grid to give BELLHOP tolerance
522 for finding solutions that otherwise may not be found in a center or single point solution.
523 The limitations of numerical computation, particularly for a complex environment, are more
524 adeptly addressed by accepting some uncertainty in position than by prescribing an exact
525 solution. Even though BELLHOP is a greedy estimator for eigenrays, the additional data
526 created is a negligible burden.
527

528 Underwater navigation research is broadly motivated by acquiring GPS-like navigation
529 accuracy in GPS-denied conditions. The Arctic, while remote, is the perfect place to test
530 mature navigation technologies in real GPS-denied conditions.

531 Range estimation is an essential step of acoustic localization and navigation. Current
532 approaches in real-time underwater acoustic navigation simplify the non-linear relationship
533 between a sound speed profile and acoustic propagation with a deterministic sound speed.
534 Some post-processing approaches attempt to leverage the acoustic arrival structure via var-
535 ious ray methods, but often use a singular SSP for simplicity, even over long term missions
536 or dynamic conditions. Thus, the conversion from travel time to range, particularly for
537 real-time vehicle deployments, can be pre-conditioned for error growth as the OWTT/range
538 increases.

539 For GPS-denied navigation, especially in hostile environments like the Arctic, tolerance
540 for error is close to none. This work addresses a critical need in acoustic navigation by

541 retooling acoustic arrival methods generally deemed too complex or labor intensive for real-
542 time, ray-based range estimation to achieve GPS-like positioning.

543 We hypothesize and validate that the embedded stochastic prediction of a single group
544 velocity is a smoothly varying function of range, source and receiver depth pairings, as
545 well as multipath structure. We employ a GPS-tracked experiment to have a ground truth
546 comparison for real-time localization algorithms. The real-time system achieves GPS-like
547 navigation for an AUV without taking into account multipath structure; the ranging error
548 improves by an order of magnitude with the suggested multipath adaptability, minimizing
549 range error to single meters. Post-processing analysis shows that this method of ranging is
550 sensitive to GPS drift itself; thus embedding a stochastic prediction of the horizontal group
551 velocity has an outsized benefit to minimizing trilateration error.

552 There are many avenues through which this approach can be further refined and tested for
553 field operations. Amongst them is defining the uncertainty grid for BELLHOP via stochastic
554 or data-driven measures such as the distance traveled by the AUV between ICNN updates
555 or the magnitude of the position corrections by the ICNN. Another is to entirely remove the
556 seeded range and instead rely on the submerged asset's depth and recorded OWTT to find
557 high probability fields in range.

558 The literature in underwater acoustic navigation and positioning is either real-time or
559 physics-based. In this paper we demonstrate a field-tested approach that is both real-time
560 and physics-based; this is achieved by coupling data streams with fast acoustic modeling.
561 The methods exploit the upward refracting nature and the total ice cover of the Arctic
562 environment to achieve remarkable ranging accuracy and precision. It transforms multipath,

563 widely considered as an obstacle for acoustic ranging, into a new information content to
 564 refine ranging accuracy. We believe that this work enables more accurate range estimation,
 565 localization, and/or navigation for any field experiment given known source and receiver
 566 depths.

567 Performance in other acoustic environments may require introducing a different thresh-
 568 olded metric to sort time of arrivals. Given the NBC algorithm's improvement with increased
 569 multipath, its effectiveness is likely only challenged by the valid operational scales of a range
 570 independent propagation environment. For mesoscale operations, like that of many glid-
 571 ers, the group velocity criteria may need to be modified to better account for variability
 572 driven by range dependent propagation through internal waves, eddies, or even bathymetric
 573 changes like underwater volcanoes. BELLHOP simulations provide other relevant eigenray
 574 information, like time and angle of arrival, that is ripe for statistical and machine learning
 575 methods to classify a representative group velocity. A bespoke and fast ray tracing method,
 576 which was used during ICEX20 to evaluate the acoustic fit of sound speed profile parame-
 577 terization ([Bhatt et al., 2022](#)), can easily report back the number of turning points instead
 578 of the number of bounces for multipath classification.

579 This approach will start to break down in extremely dynamic environments, like fast
 580 moving fronts. Realistic *in situ* considerations of the acoustic environment may not be pos-
 581 sible without complete through-the-sensor integration of acoustic dat and/or hyper realistic
 582 ocean models.

583 Many approaches to underwater navigation combine it with acoustic tomography, i.e.,
 584 a joint estimation of both source and receiver locations and the ocean volume between

them. There has been considerable success at this effort in post-processing methods, which utilize intensive—and due to the non-linearity of sound propagation, often brute force—computational methods. For vehicle operations, fast tomography is the ideal implementation, in that one can fully consider how sound speed structure, horizontally and vertically, influences sound propagation. AUVs can serve as moving sources to better image the ocean volume (Deffenbaugh, 1997; Elisseeff *et al.*, 2002), where mobile tomography and navigation converge on the same set of component technologies: position estimation, sound speed parameterization estimation, ray path identification, and vehicle path optimization.

But there are overwhelming challenges, operationally and computationally, for fast, mobile tomography to become a realistic endeavor. Addressing the spatial and temporal scales of what can be solved deterministically and what must be solved stochastically imposes a resolution constraint on the utility of gridded models—resolving fine features inaccurately (or with a false sense of confidence) could be more harmful than assuming range independence. Given that AUV operations are often on small spatial and temporal scales, the added benefit of a gridded model is quite small, and in cases like the Arctic, may actually mischaracterize the ocean volume. For gliders, with longer and larger operational scales, an ocean model may provide more useful information. Currently gliders are low power and do not have the storage or computational power to run a full-scale, realistic ocean model. A lightweight representation of the key environmental and acoustic features, passed through the same manner of acoustic message from the modem experiment, may drastically improve glider navigation.

606 **ACKNOWLEDGMENTS**

607 We acknowledge the significant operational effort spearheaded by the LAMSS ICEX20
 608 team and all our collaborators. Bhatt was funded by a National Defense, Science, and
 609 Engineering Graduate Fellowship. This work was supported by the Office of Naval Research
 610 322-OA under ICEX20 (N00014-17-1-2474) and Task Force Ocean (N00014-19-1-2716).

611

612 Ballard, M. S., Badiey, M., Sagers, J. D., Colosi, J. A., Turgut, A., Pecknold, S., Lin, Y.-T.,
 613 Proshutinsky, A., Krishfield, R., Worcester, P. F., and Dzieciuch, M. A. (**2020**). “Tem-
 614 poral and spatial dependence of a yearlong record of sound propagation from the Canada
 615 Basin to the Chukchi Shelf,” The Journal of the Acoustical Society of America **148**(3),
 616 1663–1680, <http://asa.scitation.org/doi/10.1121/10.0001970http://files/814/>
 617 [Ballardetal.-2020-Temporalandspatialdependenceofayearlongreco.pdf](#), doi: [10.1121/10.0001970](https://doi.org/10.1121/10.0001970).

618
 619 Barker, L. D. L., Jakuba, M. V., Bowen, A. D., German, C. R., Maksym, T., Mayer,
 620 L., Boetius, A., Dutrieux, P., and Whitcomb, L. L. (**2020**). “Scientific challenges and
 621 present capabilities in underwater robotic vehicle design and navigation for oceanographic
 622 exploration under-ice,” Remote Sensing **12**(16), 1–31, doi: [10.3390/RS12162588](https://doi.org/10.3390/RS12162588).

623 Bellingham, J., Leonard, J., Vaganay, J., Goudey, C., Atwood, D., Consi, T., Bales, J.,
 624 Schmidt, H., and Chryssostomidis, C. (**1995**). “Auv operations in the arctic,” in *Sea Ice
 625 Mechanics and Arctic Modeling Workshop*.

- 626 Bhatt, E. C. (2021). “A Virtual Ocean framework for environmentally adaptive, em-
 627 bedded acoustic navigation on autonomous underwater vehicles,” Ph.D. thesis, Mas-
 628 sachusetts Institute of Technology and Woods Hole Oceanographic Institution Joint Pro-
 629 gram, <https://hdl.handle.net/1912/27309>, doi: [10.1575/1912/27309](https://doi.org/10.1575/1912/27309).
- 630 Bhatt, E. C., Howard, B., and Schmidt, H. (2022). “An Embedded Tactical Decision Aid
 631 Framework for Environmentally Adaptive Autonomous Underwater Vehicle Communica-
 632 tion and Navigation,” IEEE Journal of Oceanic Engineering .
- 633 Brooke, J. (1981). “Arcs (autonomous remotely controlled submersible),” in *Proceedings of*
 634 *the 1981 2nd International Symposium on Unmanned Untethered Submersible Technology*,
 635 IEEE, Vol. 2, pp. 28–28.
- 636 Chassignet, E. P., Hurlburt, H. E., Smedstad, O. M., Halliwell, G. R., Hogan, P. J., Wall-
 637 craft, A. J., Baraille, R., and Bleck, R. (2007). “The HYCOM (HYbrid Coordinate
 638 Ocean Model) data assimilative system,” Journal of Marine Systems **65**(1-4), 60–83, doi:
 639 [10.1016/J.JMARSYS.2005.09.016](https://doi.org/10.1016/J.JMARSYS.2005.09.016).
- 640 Chen, R., Poulsen, A., and Schmidt, H. (2019). “Spectral, spatial, and tem-
 641 poral characteristics of underwater ambient noise in the Beaufort Sea in 1994
 642 and 2016,” The Journal of the Acoustical Society of America **145**(2), 605–
 643 614, <https://asa.scitation.org/doi/full/10.1121/1.5088601http://files/757/>
 644 [Chenetal.-2019-Spectral,spatial,andspacecharacteristicsof.pdf](https://files/757/Chenetal.-2019-Spectral,spatial,andspacecharacteristicsof.pdf), doi: [10.1121/1.5088601](https://doi.org/10.1121/1.5088601).
- 645 Chen, R., and Schmidt, H. (2020). “Temporal and spatial charac-
 646 teristics of the Beaufort Sea ambient noise environment,” The Jour-
 647

- 648 nal of the Acoustical Society of America **148**(6), 3928–3941, <https://doi.org/10.1121/10.0002955>
- 649 //asa.scitation.org/doi/full/10.1121/10.0002955http://files/755/
- 650 [ChenandSchmidt-2020-TemporalandspatialcharacteristicsoftheBeaufou.pdf](#), doi:
- 651 [10.1121/10.0002955](https://doi.org/10.1121/10.0002955).
- 652 Claus, B., Kepper, J. H., Suman, S., and Kinsey, J. C. (2018). “Closed-loop one-way-travel-
- 653 time navigation using low-grade odometry for autonomous underwater vehicles,” Journal
- 654 of Field Robotics **35**(4), 421–434, doi: [10.1002/rob.21746](https://doi.org/10.1002/rob.21746).
- 655 Council, N. R. (2011). *National Security Implications of Climate Change for U.S. Naval Forces* (The National Academies Press, Washington, DC), <https://www.nap.edu/catalog/12914/national-security-implications-of-climate-change-for-us-naval-forces>.
- 656
- 657
- 658
- 659 Deffenbaugh, M. (1997). “Optimal Ocean Acoustic Tomography and Navigation with Mov-
- 660 ing Sources,” Ph.D. thesis, MIT-WHOI Joint Program in Oceanography/Applied Ocean
- 661 Science and Engineering.
- 662 Deffenbaugh, M., Bellingham, J. G., and Schmidt, H. (1996a). “Relationship between
- 663 spherical and hyperbolic positioning,” Oceans Conference Record (IEEE) **2**, 590–595, doi:
- 664 [10.1109/OCEANS.1996.568293](https://doi.org/10.1109/OCEANS.1996.568293).
- 665 Deffenbaugh, M., Schmidt, H., and Bellingham, J. G. (1996b). “Acoustic positioning in a
- 666 fading multipath environment,” in *OCEANS 96 MTS/IEEE Conference Proceedings. The*
- 667 *Coastal Ocean-Prospects for the 21st Century*, IEEE, Vol. 2, pp. 596–600.
- 668 Duda, T. F., Morozov, A. K., Howe, B. M., Brown, M. G., Speer, K., Lazarevich,
- 669 P., Worcester, P. F., and Cornuelle, B. D. (2006). “Evaluation of a long-range joint

- 670 acoustic navigation / thermometry system," in *Oceans 2006*, pp. 1–6, <http://files/939/Dudaetal.-2006-EvaluationofaLong-RangeJointAcousticNavigati.pdf> <http://files/940/4099137.html>, doi: [10.1109/OCEANS.2006.306999](https://doi.org/10.1109/OCEANS.2006.306999).
- 673 Duda, T. F., Zhang, W. G., and Lin, Y.-T. (2021). "Effects of Pacific Summer Water layer
 674 variations and ice cover on Beaufort Sea underwater sound ducting," *The Journal of the
 675 Acoustical Society of America* **149**(4), 2117–2136, doi: [10.1121/10.0003929](https://doi.org/10.1121/10.0003929).
- 676 Duda, T. F., Zhang, W. G., Lin, Y.-T., and Newhall, A. E. (2019). "Long-
 677 range sound propagation in the Canada Basin," <http://files/565/Dudaetal.-Unknown-LONG-RANGESOUNDPROPAGATIONINTHECANADABASIN.pdf>.
- 679 Elisseeff, P., Schmidt, H., and Xu, W. (2002). "Ocean acoustic tomography as a data assimilation problem," *IEEE Journal of Oceanic Engineering* **27**(2), 275–282, <http://files/438/Elisseeff,Schmidt,Xu-2002-OceanAcousticTomographyasaDataAssimilationProblem.pdf>, doi: [10.1109/JOE.2002.1002482](https://doi.org/10.1109/JOE.2002.1002482).
- 684 Eustice, R. M., Whitcomb, L. L., Singh, H., and Grand, M. (2006). "Recent advances in
 685 synchronous-clock one-way-travel-time acoustic navigation," *Oceans 2006* doi: [10.1109/OCEANS.2006.306931](https://doi.org/10.1109/OCEANS.2006.306931).
- 687 Eustice, R. M., Whitcomb, L. L., Singh, H., and Grund, M. (2007). "Experimental results in synchronous-clock one-way-travel-time acoustic navigation for autonomous underwater vehicles," in *Proceedings - IEEE International Conference on Robotics and Automation*, pp. 4257–4264, <http://files/877/Eusticeetal.-2007-ExperimentalResultsinSynchronous-ClockOne-Way-.pdf> <http://files/877/Eusticeetal.-2007-ExperimentalResultsinSynchronous-ClockOne-Way-.pdf>

- 692 <http://files/878/4209752.html>, doi: [10.1109/ROBOT.2007.364134](https://doi.org/10.1109/ROBOT.2007.364134).
- 693 Fossum, T. O., Norgren, P., Fer, I., Nilsen, F., Koenig, Z. C., and Ludvigsen, M. (2021).
- 694 “Adaptive sampling of surface fronts in the arctic using an autonomous underwater ve-
- 695 hicle,” IEEE Journal of Oceanic Engineering **46**(4), 1155–1164, doi: [10.1109/JOE.2021.3070912](https://doi.org/10.1109/JOE.2021.3070912).
- 696
- 697 Freitag, L., Ball, K., Partan, J., Koski, P., and Singh, S. (2016). “Long range acoustic
- 698 communications and navigation in the Arctic,” OCEANS 2015 - MTS/IEEE Washington
- 699 2–6, doi: [10.23919/oceans.2015.7401956](https://doi.org/10.23919/oceans.2015.7401956).
- 700 Graupe, C. E., Van Uffelen, L. J., Webster, S. E., Worcester, P. F., and Dzieci-
- 701 uch, M. A. (2019). “Preliminary results for glider localization in the Beau-
- 702 fort Duct using broadband acoustic sources at long range,” in *OCEANS 2019*
- 703 *MTS/IEEE Seattle, OCEANS 2019*, pp. 1–6, <http://files/763/Graupeetal.-2019-Preliminaryresultsforgliderlocalizationinthe.pdf>
- 704 <http://files/763/Graupeetal.-2019-Preliminaryresultsforgliderlocalizationinthe.pdf>
- 705 <http://files/912/>
- 706 <http://files/764/8962637.html> <http://files/913/8962637.html>, doi: [10.23919/OCEANS40490.2019.8962637](https://doi.org/10.23919/OCEANS40490.2019.8962637).
- 707
- 708 Hayes, D. R., and Morison, J. H. (2002). “Determining turbulent vertical velocity, and
- 709 fluxes of heat and salt with an autonomous underwater vehicle,” Journal of Atmospheric
- 710 and Oceanic Technology **19**(5), 759–779.
- 711 Howe, B. M., Miksis-Olds, J., Rehm, E., Sagen, H., Worcester, P. F., and Haral-
- 712 abus, G. (2019). “Observing the Oceans Acoustically,” Frontiers in Marine Science **6**,
- 713 426, <https://www.frontiersin.org/article/10.3389/fmars.2019.00426/full>, doi:

714 10.3389/fmars.2019.00426.

715 Jackson, E. (1983). “Autonomous remotely controlled submersible “ARCS”,” in *Proceedings
716 of the 1983 3rd International Symposium on Unmanned Untethered Submersible Technol-
717 ogy*, IEEE, Vol. 3, pp. 77–88.

718 Jakuba, M. V., Roman, C. N., Singh, H., Murphy, C., Kunz, C., Willis, C., Sato,
719 T., and Sohn, R. A. (2008). “Long-baseline acoustic navigation for under-ice
720 autonomous underwater vehicle operations,” *Journal of Field Robotics* **25**(11-12),
721 861–879, <https://onlinelibrary.wiley.com/doi/full/10.1002/rob.20250>
722 <https://onlinelibrary.wiley.com/doi/abs/10.1002/rob.20250>
723 <https://wiley.com/doi/10.1002/rob.20250>, doi: 10.1002/ROB.20250.

724 Kepper, J. H., Claus, B. C., and Kinsey, J. C. (2017). “MEMS IMU and one-
725 way-travel-time navigation for autonomous underwater vehicles,” in *OCEANS
726 2017 - Aberdeen*, Vol. 2017-Octob, pp. 1–9, <http://files/550/Kepper,Claus,Kinsey-2017-MEMSIMUandOne-Way-Travel-TimeNavigationforAutonomousUnderwaterVehicles.pdf>,
727 doi: 10.1109/OCEANSE.2017.8084842.

729 Krishfield, R., Toole, J., Proshutinsky, A., and Timmermans, M. L. (2008). “Automated
730 ice-tethered profilers for seawater observations under pack ice in all seasons,” *Journal of
731 Atmospheric and Oceanic Technology* **25**(11), 2091–2105, doi: 10.1175/2008JTECH0587.
732 1.

733 Kukulya, A., Plueddemann, A., Austin, T., Stokey, R., Purcell, M., Allen, B., Littlefield, R.,
734 Freitag, L., Koski, P., Gallimore, E. et al. (2010). “Under-ice operations with a remus-100
735 auv in the arctic,” in *2010 IEEE/OES Autonomous Underwater Vehicles*, IEEE, pp. 1–8.

- 736 Kunz, C., Murphy, C., Camilli, R., Singh, H., Bailey, J., Eustice, R., Jakuba, M., Nakamura,
 737 K., Roman, C., Sato, T., Sohn, R., and Willis, C. (2008). “Deep sea underwater robotic
 738 exploration in the ice-covered Arctic ocean with AUVs,” in *2008 IEEE/RSJ International
 739 Conference on Intelligent Robots and Systems*, IEEE, pp. 3654–3660, <http://files/875/Kunzetal.-2008-Deepseaunderwaterroboticexplorationintheice.pdf>
 740 <http://files/968/Kunzetal.-2008-Deepseaunderwaterroboticexplorationintheice.pdf>
 741 <http://ieeexplore.ieee.org/document/4651097/>, doi: [10.1109/IROS.2008.4651097](https://doi.org/10.1109/IROS.2008.4651097).
- 742 Light, R., and Morison, J. (1989). “The autonomous conductivity-temprtture vehicle: First
 743 in the seashuttle family of autonomous underwater vehicle’s for scientific payloads,” in
 744 *Proceedings OCEANS*, Vol. 3, pp. 793–798, doi: [10.1109/OCEANS.1989.586683](https://doi.org/10.1109/OCEANS.1989.586683).
- 745 Litvak, A. (2015). “Acoustics of the deepwater part of the arctic ocean and of russia’s
 746 arctic shelf,” Herald of the Russian Academy of Sciences **85**, 239–250, doi: [10.1134/S1019331615030144](https://doi.org/10.1134/S1019331615030144).
- 747 Mikhalevsky, P. N., Sperry, B. J., Woolfe, K. F., Dzieciuch, M. A., and Worces-
 748 ter, P. F. (2020). “Deep ocean long range underwater navigation,” The Jour-
 749 nal of the Acoustical Society of America **147**(4), 2365–2382, <http://asa.scitation.org/doi/10.1121/10.0001081>
 750 <http://files/631/Mikhalevskyetal.-2020-Deepoceanlongrangeunderwaternavigation.pdf>, doi: [10.1121/10.0001081](https://doi.org/10.1121/10.0001081).
- 751 Norgren, P., Lubbad, R., and Skjetne, R. (2014). “Unmanned underwater vehicles in Arctic
 752 operations,” in *22nd IAHR International Symposium on Ice*.

- 757 Paull, L., Saeedi, S., Seto, M., and Li, H. (2014). *AUV navigation and*
 758 *localization: A review*, **39**, pp. 131–149, <http://files/127/Paulletal.-2014-AUVnavigationandlocalizationAreview.pdf>.
- 760 Plueddemann, A. J., Kukulya, A. L., Stokey, R., and Freitag, L. (2012). “Autonomous
 761 Underwater Vehicle Operations Beneath Coastal Sea Ice,” IEEE/ASME Transactions
 762 on Mechatronics **17**(1), 54–64, doi: [10.1109/TMECH.2011.2174798](https://doi.org/10.1109/TMECH.2011.2174798) conference Name:
 763 IEEE/ASME Transactions on Mechatronics.
- 764 Porter, M. B. (2011). “The BELLHOP Manual and User’s Guide,” HLS Research, , 2010
 765 1–57, <http://oalib.hlsresearch.com/Rays/HLS-2010-1.pdf>.
- 766 Poulsen, A. J., and Schmidt, H. (2017). “Acoustic noise properties in the rapidly changing
 767 Arctic Ocean,” **070005**(2016), 070005, doi: [10.1121/2.0000552](https://doi.org/10.1121/2.0000552).
- 768 Randeni, S., Schneider, T., and Schmidt, H. (2020). “Construction of a
 769 high-resolution under-ice AUV navigation framework using a multidisci-
 770 plinary virtual environment,” in *2020 IEEE/OES Autonomous Underwater
 771 Vehicles Symposium, AUV 2020*, pp. 1–7, <http://files/689/Randenietal.-2020-Constructionofahigh-resolutionunder-iceAUVna.pdf>, doi: [10.1109/AUV50043.2020.9267950](https://doi.org/10.1109/AUV50043.2020.9267950).
- 772
- 773
- 774 Randeni, S., Schneider, T., Schmidt, H., Bhatt, E., and Viquez, O. (2021). “A high-
 775 resolution AUV navigation framework with integrated communication and tracking for
 776 under-ice deployments,” *Field Robotics* (in review).
- 777 Rossby, T., Dorson, D., and Fontaine, J. (1986). “The RAFOS System,” *Journal of Atmo-*
 778 *spheric and Oceanic Technology* **3**, 148–162.

- 779 Rypkema, N. R., Fischell, E. M., and Schmidt, H. (2017). “One-Way Travel-Time Inverted
 780 Ultra-Short Baseline Localization for Low-Cost Autonomous Underwater Vehicles,” in *2017*
 781 *IEEE International Conference on Robotics and Automation (ICRA)*, Singapore, pp. 4920–
 782 4926.
- 783 Schmidt, H., and Schneider, T. (2016). “Acoustic communication and navigation in
 784 the new Arctic-A model case for environmental adaptation,” 3rd Underwater Com-
 785 munications and Networking Conference, Ucomms 2016 <http://files/583/Schmidt,Schneider-2016-AcousticCommunicationandNavigationintheNewArctic-AModelCaseforEnvironment.pdf>, doi: [10.1109/UComms.2016.7583469](https://doi.org/10.1109/UComms.2016.7583469).
- 786 Schneider, T., and Schmidt, H. (2018). “NETSIM: A realtime virtual ocean hardware-
 787 in-the-loop acoustic modem network simulator,” in *2018 4th Underwater Communi-
 788 cations and Networking Conference, UComms 2018*, pp. 1–5, <http://files/1047/SchneiderandSchmidt-2018-NETSIMARealtimeVirtualOceanHardware-in-the-l.pdf>, doi: [10.1109/UComms.2018.8493188](https://doi.org/10.1109/UComms.2018.8493188).
- 789 Schneider, T., Schmidt, H., and Randeni, S. (2020). “Self-Adapting Under-Ice Inte-
 790 grated Communications and Navigation Network,” 2020 5th Underwater Communica-
 791 tions and Networking Conference, UComms 2020 5, <http://files/607/Schneideretal.-Self-AdaptingUnder-IceIntegratedCommunications.pdf>.
- 792 Singh, S., Grand, M., Bingham, B., Eustice, R., Singh, H., and Freitag, L. (2006).
 793 “Underwater acoustic navigation with the WHOI Micro-Modem,” in *Oceans 2006*,
 794 IEEE, pp. 1–4, <http://ieeexplore.ieee.org/document/4099008/>, doi: [10.1109/OCEANS.2006.1700001](https://doi.org/10.1109/OCEANS.2006.1700001).
 795 Singh et al. - 2006 - Underwater Acoustic Navigation with the WHOI Micro.pdf

801 1109/OCEANS.2006.306853.

802 Timmermans, M.-L., and Winsor, P. (2013). “Scales of horizontal density structure in the
803 chukchi sea surface layer,” Continental Shelf Research **52**, 39–45.

804 Toole, J. M., Krishfield, R. A., Timmermans, M. L., and Proshutinsky, A. (2011). “The
805 Ice-Tethered profiler: Argo of the Arctic,” Oceanography **24**(3), 126–135, doi: [10.5670/oceanog.2011.64](https://doi.org/10.5670/oceanog.2011.64).

807 Uffelen, L. J. V., Howe, B. M., Nosal, E.-M., Carter, G. S., Worcester, P. F., and Dzieci-
808 uch, M. A. (2016). “Localization and subsurface position error estimation of gliders using
809 broadband acoustic signals at long range,” IEEE Journal of Oceanic Engineering **41**(3),
810 501–508.

811 Van Uffelen, L. J. (2021). “Global Positioning Systems: Over Land and Under Sea,” Acous-
812 tics Today **17**(1), 52, doi: [10.1121/at.2021.17.1.52](https://doi.org/10.1121/at.2021.17.1.52).

813 Van Uffelen, L. J., Nosal, E.-M., Howe, B. M., Carter, G. S., Worcester, P. F., Dzieciuch,
814 M. A., Heaney, K. D., Campbell, R. L., and Cross, P. S. (2013). “Estimating uncertainty
815 in subsurface glider position using transmissions from fixed acoustic tomography sources,”
816 The Journal of the Acoustical Society of America **134**(4), 3260–3271, doi: [10.1121/1.4818841](https://doi.org/10.1121/1.4818841).

818 Webster, S. E., Eustice, R. M., Singh, H., and Whitcomb, L. L. (2009). “Prelim-
819 inary deep water results in single-beacon one-way-travel-time acoustic navigation
820 for underwater vehicles,” 2009 IEEE/RSJ International Conference on Intelligent
821 Robots and Systems, IROS 2009 2053–2060, <http://files/416/Websteretal.-2009-Preliminarydeepwaterresultsinsingle-beaconone-way-travel-timeacousticnavigationf>

- 823 pdf, doi: [10.1109/IROS.2009.5354457](https://doi.org/10.1109/IROS.2009.5354457).
- 824 Webster, S. E., Eustice, R. M., Singh, H., and Whitcomb, L. L. (2012). “Advances in
 825 single-beacon one-way-travel-time acoustic navigation for underwater vehicles,” Interna-
 826 tional Journal of Robotics Research **31**(8), 935–950, doi: [10.1177/0278364912446166](https://doi.org/10.1177/0278364912446166).
- 827 Webster, S. E., Freitag, L. E., Lee, C. M., and Gobat, J. I. (2015). “Towards real-time
 828 under-ice acoustic navigation at mesoscale ranges,” in *Proceedings - IEEE International
 829 Conference on Robotics and Automation*, June, IEEE, pp. 537–544, [http://files/625/
 830 Websteretal.-2015-Towardsreal-timeunder-iceacousticnavigationat.pdf](http://files/625/Websteretal.-2015-Towardsreal-timeunder-iceacousticnavigationat.pdf)
 831 <http://files/641/Websteretal.-2015-Towardsreal-timeunder-iceacousticnavigationat.pdf>
- 832 http://files/835/Websteretal.-2015-Towardsreal-timeunde, doi: [10.1109/ICRA.2015.7139231](https://doi.org/10.1109/ICRA.2015.7139231).
- 834 Wu, M., Barmin, M. P., Andrew, R. K., Weichman, P. B., White, A. W., Lavely, E. M.,
 835 Dzieciuch, M. A., Mercer, J. A., Worcester, P. F., and Ritzwoller, M. H. (2019).
 836 “Deep water acoustic range estimation based on an ocean general circulation model:
 837 Application to PhilSea10 data,” The Journal of the Acoustical Society of America
 838 **146**(6), 4754–4773, [https://asa.scitation.org/doi/10.1121/1.5138606](https://doi.org/10.1121/1.5138606)
 839 <http://files/947/Wuetal.-2019-Deepwateracousticrangeestimationbasedonano.pdf>
 840 <http://files/948/1.html>, doi: [10.1121/1.5138606](https://doi.org/10.1121/1.5138606).